Mathematical modelling of the use of macrophages as vehicles for drug-delivery to hypoxic tumour sites

MARKUS R OWEN[1], HELEN M BYRNE[2] AND CLAIRE E LEWIS[3]

[1] Mathematical Biology Group, Department of Mathematical Sciences, Loughborough University, Loughborough, LE11 3TU, UK.
M.R.Owen@lboro.ac.uk

[2] Centre for Mathematical Medicine, School of Mathematical Sciences, University of Nottingham, Nottingham, NG7 2RD, UK.
Helen.Byrne@nottingham.ac.uk

[3] Tumour Targeting Group, Division of Genomic Medicine, University of Sheffield Medical School, Beech Hill Road, Sheffield S10 2RX, UK.
Claire.Lewis@sheffield.ac.uk

Abstract

Poor drug delivery and low rates of cell proliferation are two factors associated with hypoxia that diminish the efficacy of many chemotherapeutic drugs. Since macrophages are known to migrate specifically towards, and localise within, hypoxic tumour regions, a promising resolution to these problems involves genetically engineering macrophages to perform such anti-tumour functions as inducing cell lysis and inhibiting angiogenesis. In this paper we outline a modelling approach to characterise macrophage infiltration into early avascular solid tumours, and extensions to study the interaction of these cells with macrophages already present within the tumour. We investigate the role of chemotaxis and chemokine production, and the efficacy of macrophages as vehicles for drug delivery to hypoxic tumour sites.

The model is based upon a growing avascular tumour spheroid, in which volume is filled by tumour cells, macrophages and extracellular material, and tumour cell proliferation and death is regulated by nutrient diffusion. Crucially, macrophages occupy volume, and hence contribute to the volume balance and hence the size of the tumour. We also include oxygen dependent production of macrophage chemokines, which can lead to accumulations in the hypoxic region of the tumour. We find that the macrophage chemotactic sensitivity is a key determinant of macrophage infiltration and tumour size. Although increased infiltration should be beneficial from the point of view of macrophage-based therapies, such infiltration in fact leads to increased tumour sizes.

Finally, we include terms representing the induced death of tumour cells by hypoxic engineered macrophages. We demonstrate that reductions in tumour size can be achieved, but predict that a combination of therapies would be required for complete eradication. We also highlight some counter-intuitive predictions—for example, absolute and relative measures of tumour burden lead to different conclusions about prognosis. In summary, this paper illustrates how mathematical models may be used to investigate promising macrophage-based therapies.

1 Introduction

A characteristic feature of many solid tumours, growing *in vivo* or as tumour spheroids *in vitro*, is the presence of regions of low oxygen or hypoxia, as evidenced by microelectrode measurements and staining for hypoxia inducible factors (Figure 1a). In avascular tumours that do not possess a blood supply, or in spheroids, cultured *in vitro*, hypoxic regions form when tumours reach a critical size when the diffusion of oxygen and other nutrients from the surrounding medium is insufficient to meet the metabolic demands of cells in the interior. The same mechanism is believed to trigger the appearance of hypoxia in vascularised tumours. Blood vessels within such tumours are typically surrounded by an annulus of proliferating cells a few cells thick, followed by a poorly oxygenated or hypoxic layer. Often there are regions beyond this which are so starved of oxygen that the cells are unable to survive and form a necrotic region (see Figure 1).

Cells respond to hypoxia in a number of ways. Typically they reduce their rates of proliferation and, hence, become less responsive to chemotherapies that target rapidly dividing cells. They may also produce a range of chemicals, including Vascular Endothelial Growth Factor (VEGF), which stimulate angiogenesis, the generation and directed migration of new blood vessels into the tumour (Maxwell et al., 1997). For these reasons the degree of hypoxia within a solid tumour often correlates with prognosis (Howell et al., 2002; Ichikura et al., 2001) and clinicians have been striving to develop novel therapies that will target hypoxic sites within tumours.

The aim of one promising therapeutic approach is to exploit the propensity of a class of white blood cells known as macrophages to accumulate in hypoxic regions (Lewis et al., 1999) (see Figure 1b), this localisation being widely attributed to increased rates of production of macrophage chemoattractants such as VEGF and Macrophage Chemoattractant Protein-1 (MCP-1) under hypoxia. The main principle of the new therapy is to equip the macrophages with therapeutic genes whose expression is induced by hypoxia (Griffiths et al., 2000). For example, a proportion of a patient's macrophages could be harvested and transduced with a gene encoding cytochrome P450 before being injected back into the patient where they aggregate preferentially in hypoxic regions. Under hypoxia the macrophages release the enzyme cytochrome P450, which activates the prodrug cyclophosphamide (injected shortly after the engineered macrophages), leading to localised tumour cell kill. Since the oxygen tensions that characterise tumour hypoxia *in vivo* are considerably lower than those found elsewhere in a patient's body, it is hoped that genetically engineered macrophages which target hypoxic regions should provide a high degree of therapeutic specificity. In so doing, the extent of undesirable side-effects such as hair loss and nausea that are often associated with chemotherapy should also be diminished.

Whilst results obtained to date using this macrophage, gene-based therapy are promising, many questions remain to be answered before the approach can be used routinely in a clinical setting. For example, before the impact of treating a tumour with engineered macrophages can be assessed, the mechanisms by which normal (*i.e.* non-engineered) macrophages accumulate in hypoxic regions must be more fully elucidated and the impact that they have on the tumour's size and structure clarified. Studies *in vitro* demonstrate that, while chemotaxis may enhance macrophage aggregation in hypoxic tumour regions, macrophages may also infiltrate into multicell spheroids in significant numbers in the absence of chemotactic stimuli (Leek, 1999). Preliminary modelling by Kelly *et al.*, designed to explain these findings, indicates that neither hypoxia nor necrosis are necessary for macrophage infiltration: macrophages can migrate towards and within tumours by random motion alone (Kelly et al., 2002). In addition, the number of infiltrating macrophages increases with tumour size for both chemoattractant-producing and chemoattractant-deficient spheroids.

The model developed in (Kelly et al., 2002) assumes that the tumour volume does not change during macrophage infiltration and neglects the volume occupied by the macrophages, even though the experimental data indicate that tumours increase in size during macrophage infiltration (Leek, 1999). In this paper we develop a mathematical model of macrophage infiltration into avascular tumours in which both of these assumptions are relaxed. This is achieved by extending the multiphase modelling framework developed by Ward and King (Ward and King, 1997; Ward and King, 1999), which accounts explicitly for the volume fractions of tumour cells and extracellular material. Related multiphase approaches have been applied to various aspects of tumour growth, including capsule formation (Jackson and Byrne, 2002; Lubkin and Jackson, 2002) and vascular tumour growth (Breward et al., 2003). Many other models have also been developed for different aspects of tumour progression, including individual-based models for avascular growth (Drasdo and Hohme, 2003) and angiogenesis (Anderson and Chaplain, 1998; Levine et al., 2001). In addition, there has been considerable work on the detailed mathematical analysis of models for tumour biology (Fontelos et al., 2002; Friedman and Reitich, 1999).

In Section 2 we develop our mathematical model for macrophage infiltration into tumours. In Section 3 we demonstrate the good agreement that may be achieved between experimental growth curves for HEPA-1 spheroids *in-vitro* and our basic tumour growth model when no macrophages are present. With this foundation, we use the full model to determine the effect of macrophage infiltration on the tumour's size and composition, *i.e.* the number of live tumour cells within the spheroid and the fraction that are proliferating. This includes a comparison of macrophage infiltration with and without macrophage chemotaxis. In Section 4, we study the effect of macrophage-dependent tumour cell killing. Another important practical question that we investigate concerns the ability of engineered macrophages to displace the normal

3

macrophages already present in hypoxic regions of tumours. We address this issue by extending our model so that it describes interactions between the tumour cells and two macrophage populations (normal and genetically engineered). Finally, in Section 5 we discuss the biological significance of our results and make a number of suggestions for future work.

2   Generalised Macrophage Infiltration Model

In this section we present a general mathematical model that describes the growth of an avascular, multicell spheroid which is being infiltrated by macrophages. We view the tumour as comprising three, key constituents, or phases, namely macrophages $l(\mathbf{x}, t)$, tumour cells $m(\mathbf{x}, t)$ and cellular material $n(\mathbf{x}, t)$. (We make no explicit mention of such components as extracellular matrix and stroma, incorporating them into our definition of cellular material.) We assume that cellular material is predominantly composed of water and is produced when tumour cells and macrophages die. It acts as a source of material for cell growth and proliferation. Other model variables that we introduce represent the oxygen concentration $c(\mathbf{x}, t)$ and a generic macrophage chemoattractant $a(\mathbf{x}, t)$. For simplicity, and in view of our focus on hypoxia, we assume that oxygen, which is supplied from the medium surrounding the spheroid, is the rate-limiting nutrient (i.e. all other nutrients, such as glucose, that are essential for cellular metabolism are abundant). We assume that the macrophage chemoattractant is produced under hypoxia by the tumour cells and macrophages. (In practice, the chemoattractant may represent VEGF, MCP-1 or one of the other chemoattractants produced under hypoxia.)

Applying the principle of mass balance to each of our variables, and introducing $\mathbf{v}(\mathbf{x}, t)$ to denote the common advection velocity with which it is assumed that all species are transported, we obtain the following system of partial differential equations which describe the evolution of l, m, n, c and a:

$$
\begin{align}
\frac{\partial l}{\partial t} &= \nabla \cdot (D_l \nabla l - \chi l \nabla a - \mathbf{v} l) - d_l(c) l, \tag{1} \\
\frac{\partial m}{\partial t} &= \nabla \cdot (D_m \nabla m - \mathbf{v} m) + p_m(n, c) m - d_m(c) m - k(c) l m, \tag{2} \\
\frac{\partial n}{\partial t} &= \nabla \cdot (D_n \nabla n - \mathbf{v} n) + d_l(c) l + d_m(c) m + k(c) l m - p_m(n, c) m, \tag{3} \\
\frac{\partial c}{\partial t} &= D_c \nabla \cdot (\nabla c - \mathbf{v} c) - d_c(l, m, c), \tag{4} \\
\frac{\partial a}{\partial t} &= D_a \nabla \cdot (\nabla a - \mathbf{v} a) + p_a(l, m, c) - d_a a. \tag{5}
\end{align}
$$

In equations (1)-(3), $D_i\,(i=l,m,n)$ denote the random motility coefficients of the three phases, and χ represents the macrophage chemotaxis coefficient; in the following, $D_i\,(i=l,m,n)$ and χ are assumed constant. This is a simplification, since hypoxia and the tumour microenvironment can alter chemokine receptor expression (Scotton et al., 2001; Sica et al., 2000), and there is also evidence that leukocyte random and chemotactic motility parameters vary with chemokine concentration (Owen and Sherratt, 1997; Sherratt, 1994; Sozzani et al., 1991). Furthermore, we omit details of the subcellular events that regulate chemoreception, such as ligand receptor binding and signal transduction (Berg and Purcell, 1977; Wiegel, 1983).

We justify the inclusion of random motion of the cellular material on the basis that it comprises water and cellular debris, and that the latter will undergo a certain, albeit small, degree of random motion. The source and sink terms that appear in equations (1)-(3) may be interpreted in the following manner. In (2), $p_m(n,c)$ denotes the rate at which the tumour cell proliferate, $d_m(c)$ represents the rate at which tumour cells die due to apoptosis and/or necrosis, when no macrophages are present, and $k(c)$ represents the oxygen-dependent rate at which macrophages kill tumour cells. In (1) we assume that, since macrophages are mature white blood cells, they do not proliferate. We assume further that they are not affected by tumour cell lysis and denote by $d_l(c)$ the oxygen-dependent rate at which they undergo natural death.

Adding equations (1)-(3), we remark that the net source term is zero and, hence, that there is no local mass creation within the tumour volume: mass is merely transformed from one phase to another. As we show below, the flux of cellular material and macrophages across the outer tumour boundary governs the rate at which the tumour volume changes (see equation (16)).

In equations (4) and (5), D_c and D_a denote the assumed constant oxygen and chemoattractant diffusion coefficients, $d_c(l,m,c)$ represents the rate at which the tumour cells and macrophages consume oxygen, $p_a(l,m,c)$ represents the rate at which they produce chemoattractant and d_a the assumed constant rate at which the chemoattractant decays (oxygen decay is neglected).

In order to complete our model, it remains to determine the advection velocity $\mathbf{v}(\mathbf{x},t)$. Following Ward and King (Ward and King, 1997; Ward and King, 1999), we assume that there are no voids within the tumour and hence that throughout the spheroid

$$l+m+n=N_0$$

where N_0 is a constant, representing the amount of cellular material contained within a unit control volume. Summing equations (1)-(3) then yields

$$N_0 \nabla . \mathbf{v} = \nabla . (D_l \nabla l - \chi l \nabla a + D_m \nabla m + D_n \nabla n). \tag{6}$$

In general, for three-dimensional spheroid growth, equations (1)-(6) are insufficient to determine the 8 variables l, m, n, a, c and $\mathbf{v}$: additional equations are needed to close the system. One possible closure involves using Darcy's law ($\mathbf{v} = -K \nabla P$) to relate the velocity to the pressure P: in this case the model comprises 9 equations for 9 variables (Greenspan, 1976). Alternative approaches, which involve employing more complex constitutive laws, are presented in (Breward et al., 2002; Byrne et al., 2002; Franks and King, 2002). In this paper, we avoid these issues by assuming that the spheroid undergoes one-dimensional, radially-symmetric growth. Then equations (1)-(6) are sufficient to determine l, m, n, a, c and $\mathbf{v}$ ($\equiv (v(r,t), 0, 0)$ under radial symmetry).

We assume that the tumour occupies the region $0 < r < R(t)$ and that the tumour boundary $r = R(t)$ delineates the region of space in which $m > 0$. We assume further that $r = R(t)$ moves with the tumour cell velocity v_m there so that, referring to (2), we have

$$\frac{dR}{dt} = v_m|_{r=R(t)} = \left[v - \frac{D_m}{m} \frac{\partial m}{\partial r} \right]_{r=R(t)}. \tag{7}$$

Thus our model of one-dimensional, radially-symmetric spheroid growth with macrophage infiltration comprises equations (1)-(7). Before specifying the kinetic terms, we present the boundary and initial conditions.

The Boundary and Initial Conditions
We assume that the tumour is symmetric about the origin so that

$$0 = \frac{\partial l}{\partial r} = \frac{\partial m}{\partial r} = \frac{\partial n}{\partial r} = \frac{\partial c}{\partial r} = \frac{\partial a}{\partial r} = v \quad \text{at } r = 0. \tag{8}$$

We denote by l_∞ and n_∞ the concentrations of macrophages and cellular material exterior to the spheroid and assume that the flux of these species across the tumour boundary is proportional to the differences $(l_\infty - l(R,t))$ and $(n_\infty - n(R,t))$ respectively. Since the tumour boundary is itself moving with velocity $v_m(R,t)$ (see equation (7)), we deduce that the appropriate flux boundary conditions on $r = R(t)$ are:

$$-l(v_l - v_m) = h_l(l_\infty - l) \quad \text{and} \quad -n(v_n - v_m) = h_n(n_\infty - n) \quad \text{on } r = R(t), \tag{9}$$

where the non-negative constants h_l and h_n represent the permeabilities of the tumour boundary to macrophages and cellular material and v_l and v_n represent the velocities of the macrophages and cellular material so that

$$v_l(R,t) = v - \frac{D_l}{l}\frac{\partial l}{\partial r} + \chi\frac{\partial a}{\partial r}\bigg|_{r=R(t)} \quad , \quad v_m(R,t) = v - \frac{D_m}{m}\frac{\partial m}{\partial r}\bigg|_{r=R(t)} \quad , \quad v_n(R,t) = v - \frac{D_n}{n}\frac{\partial n}{\partial r}\bigg|_{r=R(t)} .$$

Substituting for v_l, v_m and v_n in (9) we obtain

$$D_l\frac{\partial l}{\partial r} - \chi l\frac{\partial a}{\partial r} - D_m\frac{l}{m}\frac{\partial m}{\partial r} = h_l(l_\infty - l) \quad \text{and} \quad D_n\frac{\partial n}{\partial r} - D_m\frac{n}{m}\frac{\partial m}{\partial r} = h_n(n_\infty - n). \quad (10)$$

We remark that since $l + m + n = N_0$ throughout the tumour, it is not necessary to impose an additional boundary condition on $r = R(t)$ for m. We note also that, in (10), l_∞ and n_∞ may be time-dependent. For example, if the spheroid is infused with macrophages for a finite period of time $(t_{on} < t < t_{off})$, then

$$l_\infty(t) = \begin{cases} l_\infty & \text{if } t_{on} < t < t_{off}, \\ 0 & \text{otherwise.} \end{cases} \quad (11)$$

Since oxygen is a small, highly diffusible molecule, we assume that the oxygen concentration on the tumour boundary is in equilibrium with that exterior to the tumour where $c = c_\infty$. Thus we fix

$$c = c_\infty \quad \text{on } r = R(t). \quad (12)$$

Denoting by h_a the permeability of the tumour boundary to the chemoattractant, which, being a larger molecule than oxygen, will diffuse less rapidly, we assume further that

$$D_a\frac{\partial a}{\partial r} - D_m\frac{a}{m}\frac{\partial m}{\partial r} = h_a(a_\infty - a) \quad \text{on } r = R(t), \quad (13)$$

where a_∞ represents the chemoattractant concentration exterior to the tumour.

We remark that in equations (10) and (13) we suppose that the permeabilities h_l, h_n and h_a are non-negative constants. More generally, since the chemoattractant is believed to enhance

the ability of macrophages to infiltrate the tumour, we might consider $h_l = h_l(a)$ where $h_l(a)$ is a monotonically decreasing function of a (Kelly, 2002).

We suppose that initially the tumour is devoid of macrophages and chemoattractant. We specify the distribution of cells, cellular material and oxygen, together with the tumour radius, at $t = 0$. Thus we have:

$$l(r, 0) = 0, \quad m(r, 0) = m_0(r), \quad n(r, 0) = 1 - m_0(r), \left. \begin{array}{c} \\ \\ \end{array} \right\}$$
$$c(r, 0) = c_0(r), \quad a(r, 0) = 0, \quad R(0) = R_0 \qquad (14)$$

where R_0 and the functions $m_0(r)$ and $c_0(r)$ are prescribed.

Before specifying the kinetic terms, we show how boundary conditions (10) and equation (6) may be used to simplify equation (7). Integrating (6) subject to (8) we have

$$v(r, t) = \frac{1}{N_0} \left(D_l \frac{\partial l}{\partial r} - \chi l \frac{\partial a}{\partial r} + D_m \frac{\partial m}{\partial r} + D_n \frac{\partial n}{\partial r} \right). \qquad (15)$$

Substituting with $v(R, t)$ in (7) then yields

$$\frac{dR}{dt} = \frac{1}{N_0} \left[D_l \frac{\partial l}{\partial r} - \chi l \frac{\partial a}{\partial r} + D_n \frac{\partial n}{\partial r} + D_m \left(1 - \frac{N_0}{m} \right) \frac{\partial m}{\partial r} \right]_{r=R}.$$

Using boundary conditions (10) and noting that $l + m + n = N_0$ we deduce that

$$\frac{dR}{dt} = \frac{1}{N_0} \left[h_l(l_\infty - l) + h_n(n_\infty - n) \right]_{r=R}. \qquad (16)$$

Henceforth we use (16) in place of (7) and remark that (16) is equivalent to prescribing

$$\frac{d}{dt} \left(\begin{array}{c} \text{tumour} \\ \text{volume} \end{array} \right) = \frac{d}{dt} \left(\frac{4}{3} \pi R^3 N_0 \right) = \int_{\theta=0}^{\pi} \int_{\phi=0}^{2\pi} [h_l(l_\infty - l) + h_n(n_\infty - n)] R^2 \sin \theta \, d\theta \, d\phi$$

$$= [h_l(l_\infty - l) + h_n(n_\infty - n)] \times (\text{surface area of tumour}).$$

Thus the rate at which the tumour volume changes is determined by the flux of macrophages and cellular material across the tumour boundary (material contained within the tumour volume can only change phase: it cannot be created or destroyed).

The Kinetic Terms

We now motivate our choice of the kinetic terms that appear in equations (1)-(5). Our philosophy is to use the simplest expressions possible in order to capture the essential behaviour of the system.

Since tumour cells require oxygen and cellular material to proliferate, we write $p_m = p_m(n, c)$ in equation (2). We assume that tumour cells proliferate at a rate which is an increasing, saturating function of c and n. In particular, when the oxygen concentration is low, the proliferation rate is proportional to c whereas when c is high (and oxygen is readily available) proliferation is limited merely by the availability of cellular material. Similarly, when the concentration of cellular material is low, proliferation is limited by its availability and when n exceeds a threshold level ($n > n_0$), proliferation is limited by oxygen availability. We introduce the non-negative constants p_m^{max}, c_p, α and $n_0 < N_0$, and, for simplicity, we write

$$p_m(n, c) = p_m^{max} S(c, c_p) \mathrm{Cap}(n/n_0) \tag{17}$$

$$\text{where} \quad S(c, c_p) = \frac{c^\alpha (c_p^\alpha + c_\infty^\alpha)}{c_\infty^\alpha (c_p^\alpha + c^\alpha)} \quad \text{and} \quad \mathrm{Cap}(x) = \min(x, 1).$$

The function $S(c, c^*)$ is a "switch", scaled so that $S(c_\infty, c_p) = 1$. Its steepness is regulated by α and it attains its half-maximal value when $c = c_p$.

We do not distinguish between apoptosis and necrosis as distinct mechanisms of cell death, assuming instead that there is a low, background level of cell death at all oxygen concentrations and that this rate increases as c decreases. We introduce the positive constants c_c and d_m^{max} and write

$$d_m(c) = d_m^{max} \left[1 - S(c, c_c) \right]. \tag{18}$$

In (18) c_c denotes the oxygen concentration at which the cell death rate is half-maximal. Similarly, in equation (1) we introduce d_l^{max} and write

$$d_l(c) = d_l^{max} \left[1 - S(c, c_c) \right]. \tag{19}$$

We now consider the tumour cell lysis term, $k(c)$. Since macrophages can be engineered to produce cytotoxic enzymes under hypoxia, we assume that $k(c)$ increases as c decreases. Following (18), we introduce k^{max} and write

$$k(c) = k^{max} \left[1 - S(c, c_p) \right], \tag{20}$$

9

We remark that since $l, m \to 0$ as $c \to 0$, $k(c)lm \to 0$ as $c \to 0$. Thus the overall lysis rate will exhibit biphasic dependence on the oxygen tension and attain its maximum value within the hypoxic region.

When specifying k^{max}, it is important to recall the two-stage manner in which the macrophage-based therapy kills the tumour cells. Under hypoxia the modified macrophages express cytochrome P450 (CYP450). The prodrug cyclophosamide (CPA), which is injected after the macrophages, is activated by CYP450 to stimulate lysis on absorption by the tumour cells. By analogy with (11), assuming that the prodrug is introduced at $t = T_{on}$, we assume $k^{max} = k^{max}(t)$ with

$$k^{max}(t) = \begin{cases} k^{max} & T_{on} < t \\ 0 & \text{otherwise.} \end{cases} \tag{21}$$

Following (20), in equations (4) and (5) we write

$$p_a(l, m, c) = [1 - S(c, c_p)] \ (p_{al}^{max} l + p_{am}^{max} m) \tag{22}$$

and

$$d_c(l, m, n) = S(c, c_c) [d_{cl}^{max} l + d_{cm}^{max} m] + d_{cp}^{max} p_m(n, c)m, \tag{23}$$

defining coefficients such as p_{al}^{max} in an obvious manner.

In (22) we have assumed that chemoattractant is produced by tumour cells and macrophages at rates which peak under hypoxia. In (23) we have assumed that nutrient is consumed by all live cells and that tumour cells consume additional nutrient in order to proliferate. For simplicity, we have also assumed that the threshold oxygen concentrations are the same for both cell types, and that the amount of chemoattractant released on cell death is negligible.

2.1 Dimensionless model and simplification

In Appendix A we recast our model in dimensionless form. We rescale lengths by the radius of a typical tumour cell, time by the doubling time of HEPA-1 cells under nutrient-rich conditions, and nutrient concentrations by the level at the spheroid surface. Under these rescalings nutrient

and chemoattractant diffusion occur on much shorter timescales than those associated with cell proliferation and movement (or advection). Consequently, the time-derivatives and advection terms in equations (4) and (5) may be neglected and a quasi-steady state approximation made (Greenspan, 1976; Kelly et al., 2002; Ward and King, 1997). Eliminating $n = 1 - l - m$, our dimensionless model reads:

$$\frac{\partial l}{\partial t} = \frac{1}{r^2}\frac{\partial}{\partial r}\left[r^2\left(D_l\frac{\partial l}{\partial r} - \chi l\frac{\partial a}{\partial r} - lv\right)\right] - d_l(c)l, \tag{24}$$

$$\frac{\partial m}{\partial t} = \frac{1}{r^2}\frac{\partial}{\partial r}\left[r^2\left(D_m\frac{\partial m}{\partial r} - mv\right)\right] + p_m(n,c)m - d_m(c)m - k(c)lm, \tag{25}$$

$$0 = \frac{1}{r^2}\frac{\partial}{\partial r}\left(r^2\frac{\partial c}{\partial r}\right) - d_c(l,m,c), \tag{26}$$

$$0 = \frac{1}{r^2}\frac{\partial}{\partial r}\left(r^2\frac{\partial a}{\partial r}\right) + d_a(p_a(l,m,c) - a), \tag{27}$$

$$\frac{dR}{dt} = [h_l(l_\infty - l) + h_n(n_\infty - 1 + m + l)]_{r=R}. \tag{28}$$

where

$$v = D_l\frac{\partial l}{\partial r} - \chi l\frac{\partial a}{\partial r} + D_m\frac{\partial m}{\partial r} - D_n\left(\frac{\partial l}{\partial r} + \frac{\partial m}{\partial r}\right). \tag{29}$$

The boundary conditions become

$$\frac{\partial l}{\partial r} = \frac{\partial m}{\partial r} = \frac{\partial c}{\partial r} = \frac{\partial a}{\partial r} = 0 \quad \text{at } r = 0, \tag{30}$$

$$D_l\frac{\partial l}{\partial r} - \chi l\frac{\partial a}{\partial r} - D_m\frac{l}{m}\frac{\partial m}{\partial r} = h_l(l_\infty - l) \quad \text{on } r = R(t), \tag{31}$$

$$-D_n\left(\frac{\partial l}{\partial r} + \frac{\partial m}{\partial r}\right) - D_m\frac{(1-l-m)}{m}\frac{\partial m}{\partial r} = h_n(n_\infty - 1 + l + m) \quad \text{on } r = R(t), \tag{32}$$

$$c = 1, \quad \frac{\partial a}{\partial r} = h_a(a_\infty - a) \quad \text{on } r = R(t), \tag{33}$$

$$l(r,0) = 0, \quad m(r,0) = m_0(r), \quad R(0) = R_0. \tag{34}$$

Our model can be generalised to study infiltration by two or more macrophage populations. For example, we would need to include two macrophage populations in order to determine whether engineered macrophages can displace normal, non-engineered macrophages in tumours that are growing *in vivo* (see section 4). In such cases, the second macrophage equation takes the same form as the original, and additional terms associated with the motility of this population appear in equation (29). Labelling the two populations l_1 and l_2, equation (28) generalises to give:

$$\frac{dR}{dt} = [h_{l1}(l_{\infty 1} - l_1) + h_{l2}(l_{\infty 2} - l_2) + h_n(n_\infty - 1 + l_1 + l_2 + m)]_{r=R}, \tag{35}$$

where $h_{l1}, h_{l2}, l_{\infty 1}(t)$ and $l_{\infty 2}(t)$ represent the permeabilities of the tumour boundary to the two macrophage populations and their concentrations in the medium surrounding the tumour (see section 4).

2.2   Parameter Values and Numerical Methods

The nondimensionalisation process used to obtain equations (24)-(33) and simulate our dimensionless model requires specification of a large number of parameters. While many of these values have been reported in the literature, others are more difficult to specify accurately. In Table 1 we summarise the parameters values we use to carry out the numerical simulations presented in sections 3 and 4. Where possible, dimensional and dimensionless values are stated, together with supporting references. We include below brief details of some of the calculations used to obtain these estimates.

A typical tumour cell doubling time of 18 hours has been estimated for HEPA-1 tumour cells undergoing exponential growth and, hence, proliferating at their maximum rate (Maxwell et al., 1997). The timescale used in our nondimensionalisation is associated with the maximum cell growth rate p_m^{max}. Thus, following (Ward and King, 1999), we estimate $p_m^{max} \sim \ln 2/18 \sim 0.924$ day^{-1}. Since these estimates are approximate, to facilitate comparison with experiments, we fix $p_m^{max} = 1$ day^{-1} so that the timescale of the simulations is in days.

We rescale lengths with the radius of a single cell, $R_m \sim 6\mu$m and estimate the initial spheroid radius by referring to experiments by Leek (Leek, 1999) in which 2000 cells were used to seed a spheroid. In this way we estimate $R_0^3 \sim 2000 R_m^3$ so that $R_0 \sim 13 R_m \sim 80\mu$m.

We constructed our numerical simulations by first mapping the problem onto a fixed domain $((r,t) \rightarrow (\rho, \tau) = (r/R(t), t))$, thereby reducing the model to a system of parabolic PDEs coupled to an ODE for the spheroid radius. The system was solved using the NAG routine `D03PHF`, because it allows for the direct coupling of parabolic PDEs with ODEs such as (28). It also allows the inclusion of the steady state equations (26,27). `D03PHF` uses a finite difference spatial discretisation and the method of lines, and integrates the resulting system of ODEs using a backward differentiation formula (BDF) or a Theta method — all the simulations presented in this paper used the BDF method.

3   Spheroid growth and infiltration of inert macrophages

In this section we neglect macrophage-mediated tumour cell death ($k(c) = 0$ in (25)) and focus on the impact that infiltration by inert (or passive) macrophages has on the spheroid's growth and composition. We present a series of numerical simulations showing how the infiltration pattern depends on the relative importance of random motion and chemotaxis as macrophage migratory mechanisms. Variations in these mechanisms may arise through differing rates of pro-

duction of macrophage chemokines (for example, C4 tumour cells do not produce VEGF (Kelly et al., 2002; Leek, 1999)) or through differing responses of macrophages to chemokines (this may vary from individual to individual, and in particular may be manipulated experimentally/clinically via insertion of additional copies of the genes encoding for specific chemokine receptors).

3.1 Macrophage-free spheroid growth

We begin by considering spheroid growth in the absence of macrophages. With $l = 0$, our model reduces to that studied by Ward and King (Ward and King, 1999). As figure 2(a) shows, initially cell proliferation occurs throughout the tumour. However, as the spheroid increases in size, nutrient levels near the centre decline and there is increased cell death. The resulting cellular material is transported towards the tumour surface, and growth saturates when $m = 1 - n_\infty$ on the tumour boundary.

We remark that the limiting behaviour of our macrophage-free model of spheroid growth depends on the system parameters that we use. For example, the simulations presented show a spheroid which evolves to a time-independent steady state. Increasing the nutrient consumption rate d_m^{max} decreases the steady state size. For other parameter values the spheroid may continue to grow, the system adopting a steady travelling wave profile. For example, as n_∞ increases the equilibrium tumour size increases, until a bifurcation to travelling wave solutions. More details and analysis of this bifurcation can be found in (Ward and King, 1999). We do not anticipate any other types of solution behaviour, even with the additional complexity of macrophages and tumour cell lysis, since the spatial structure of the system is dominated by the nutrient profile.

In figure 2(b) we compare our numerical simulations with experiments in which HEPA-1 spheroids were grown *in vitro* (Leek, 1999). Two types of measurement were made, *in vitro* and after fixing, sectioning and staining. The latter type allows the necrotic region to be identified and measured, but the process causes the spheroid to shrink by approximately 25% (Leek, 1999). The values used in the figure are scaled accordingly, to allow for comparison with the *in vitro* measurements and our model results. The good agreement between the experimental and numerical results for both the outer spheroid radius and the locus of the necrotic boundary suggests that our model provides a reasonable description of spheroid growth and, as such, is a sound basis for our studies of macrophage infiltration. We remark that in our simulations the necrotic and hypoxic boundaries are defined implicitly, as contours of c on which $c = c_p$ and $c = c_c$ respectively. When other criteria were used to determine these boundaries (e.g. contours

of the tumour cell density) the agreement between the numerical simulations and experimental results was less good.

3.2 Macrophage infiltration by random motion alone

In practice, not all tumour cell lines produce macrophage chemoattractants (Kelly et al., 2002; Leek, 1999). In order to test whether chemoattractant production is necessary for macrophage localisation within hypoxic regions, we performed simulations in which chemotaxis was neglected and the macrophages migrated by random motion alone. The results, which are presented in figure 3(a), show the macrophages accumulating predominantly near the tumour boundary and, to a lesser extent, in the hypoxic region.

The limiting size of the spheroid when it is infiltrated by inert macrophages depends on the parameter values associated with the macrophages. Thus, comparing figures 2(a) and 3(a) we note that the spheroid decreases in size when the inert macrophages are introduced. This is because, when the macrophages migrate by random motion alone, they compete for space with tumour cells in the outer, nutrient-rich parts of the spheroid, thereby reducing the spheroid's overall growth rate (we assume that the macrophages do not proliferate and that they die at the same rate as the tumour cells). However if the death rate of the macrophages (d_l^{max}) is reduced sufficiently (e.g. $d_l^{max} = 1.3$) then the limiting size of the spheroid is larger when macrophages are present.

3.3 Macrophage infiltration by random motion and chemotaxis

The results presented in figure 3(b) show that significant macrophage localisation within the hypoxic region can be achieved when chemotaxis operates. Comparing figures 3 (a) and (b) we observe that with chemotaxis more macrophages infiltrate the tumour and its proliferating rim is thinner.

From a therapeutic viewpoint, it is of interest to consider whether macrophages displace tumour cells in hypoxic regions: if all the tumour cells are displaced, the therapeutic value of engineering macrophages to kill tumour cells under hypoxia may be compromised. The results presented in figure 3(b) indicate that if the tumour cells are the sole source of chemoattractant then some tumour cells remain in the hypoxic region (recall that at this stage our macrophages are passive and do not kill tumour cells). In practice, it is likely that once they reach hypoxic regions the macrophages will also produce chemoattractant. Further simulations (not shown) demonstrate

that macrophage infiltration and localisation is enhanced when both the tumour cells and the macrophages produce chemoattractant. A local minimum in the tumour cell population is evident in the hypoxic region, the tumour cells having been displaced by macrophages.

3.4   Summary

Before considering how macrophage-mediated tumour cell kill influences the spheroid's growth, we place the above results in context. In order to do this, it is useful to know the total flux of macrophages, $J_{tot}(t)$ say, that have migrated into the spheroid at a prescribed time, t. Using (24) and (31) we deduce that

$$J_{tot}(t) = 4\pi \int_0^t h_l [l_\infty - l(R(\tau), \tau)] R^2(\tau) d\tau.$$

Referring to figure 4 we note firstly that when passive macrophages infiltrate by random motion and chemotaxis the spheroid's size increases markedly (compare (1) and (3) in figure 4). Since the spheroid size increases further when the macrophage death rate is reduced (compare (4) and (5) in figure 4), we deduce that the increase in size is not simply due to macrophage death providing an extra source of cellular material for tumour cell proliferation.

While the number of infiltrating macrophages undoubtedly contributes to the increase in spheroid size described above, the middle panels of figure 4 show that the number of tumour cells also increase. These results, taken in isolation, suggest that the presence of macrophages is deleterious, causing the tumour burden to increase. However, by calculating the proportion of the spheroid occupied by tumour cells and macrophages a different picture emerges. Referring to the botton panels in figure 4 we see that the proportion of the spheroid occupied by tumour cells actually decreases and that the macrophages displace the tumour cells from the hypoxic region. In this way, we might infer that the macrophages have diluted or weakened the tumour. In summary, when studying the impact on spheroid growth of infiltration by inert macrophages, care should be taken to ensure that any predictions or results are stated as clearly as possible and that potential ambiguities are highlighted.

4   Macrophage-dependent tumour cell killing

In this section we concentrate on the role of macrophage-induced tumour cell lysis, assuming that both macrophage motility mechanisms are active. Initially we consider infiltration by

a single population of engineered macrophages. In order to replicate the situation that is likely to arise when engineered macrophages are used to target tumours growing *in vivo*, we then consider infiltration by two populations of macrophages: in this case, the infiltration of a population of passive (or non-engineered) macrophages is interrupted by a population of engineered macrophages infiltrating for a finite period.

4.1 Infiltration by a single population of engineered macrophages

The results presented in figure 5 show how a spheroid shrinks when it is continuously infused with engineered macrophages for $t \geq 10$ and macrophage-mediated cell death commences when the prodrug is administered, at $t = 12$. When the macrophages reach the hypoxic region ($t \sim 15$) there is a rapid reduction in the tumour's volume ($15 < t < 20$). Thereafter the macrophages dominate the hypoxic region and the spheroid evolves to an equilibrium structure in which the tumour cells are localised on the periphery, where they will be more vulnerable to other treatments (e.g. chemotherapy) that target rapidly proliferating cells.

The reduction in spheroid size is dependent on initial conditions and the timing of macrophage and prodrug administration, since it is in fact the steady state size that is reduced. Thus, if treatment is applied sufficiently early the spheroid will simply grow more slowly than without treatment, rather than actually shrinking. This slower growth is still a beneficial outcome, and hence it may be more appropriate to consider the ratio of sizes for treated and untreated spheroids at a given time.

In practice both the number of infiltrating macrophages (l_∞) and the rate at which they kill tumour cells (k^{max}) can be manipulated. Different tumours will express different chemokines, and some may express none at all, so macrophage chemotaxis will also vary. Furthermore, it is expected that the macrophage chemotaxis coefficient (χ) can be modulated by inserting extra copies of genes coding for chemokine receptors into the engineered macrophages. In figure 6 we show how the spheroid's size and composition change as χ and k^{max} vary (see (21 and (25)). There is a marked reduction in spheroid size as k^{max} increases. While the tumour is never completely eliminated by the macrophages, for sufficiently large values of k^{max} the proportion of the spheroid occupied by tumour cells is negligible: the macrophages constitute most of its volume (data not shown). Additionally, we observe that as k^{max} increases the corresponding reduction in tumour volume declines. Indeed the reduction in tumour volume as k^{max} increases from $k^{max} = 8$ to $k^{max} = 10$ is negligible. Thus we conclude that there may be a natural upper limit to k^{max} such that further increases will not yield large enough reductions in tumour size to justify their use. Interestingly, increasing χ actually increases the spheroid size due to the

space occupied by the additional infiltration of macrophages. However, the right hand panel of figure 6 shows that the fractional reduction in tumour size is in fact enhanced with increasing χ. As noted above, for large lysis rates macrophages constitute most of the spheroid volume, and as such are relatively homogeneously distributed, so that it makes little difference if macrophage motility is predominantly random or chemotactic. Further simulations (not shown) demonstrate that, for smaller lysis rates, if macrophages are longer lived (either intrinsically, or because they are better able to tolerate hypoxia) then chemotactically aggregating macrophages outperform those which only move randomly. Varying the surface level of macrophages has the expected effect on these results – decreasing l_∞ leads to reduced infiltration and reduced tumour cell lysis.

As with existing cancer treatments, it may not be practical to infuse the tumour with a continuous supply of macrophages. Therefore, in figure 7(a) we assume that the macrophages are applied for a finite period of time ($10 < t < 12$). For comparison with figure 5 we suppose that the macrophage-mediated cell kill is initiated at $t = 12$, so that $T_{on} = 12$ in equation (21). The macrophages migrate towards the hypoxic region and the spheroid shrinks until the macrophage level there declines and growth resumes. When macrophages move only randomly, the initial infiltration is concentrated at the tumour surface, but then the majority of those macrophages are advected into the spheroid, inducing tumour cell lysis as they go. For this reason, the effect of such macrophages is comparable to those which chemotactically aggregate. However, in a similar manner to that described above for continuous infiltration, if macrophages are longer lived then chemotaxis results in a greater reduction in tumour size (data not shown).

4.2   Multiple macrophage populations

As stated above, when assessing the impact of genetically engineered macrophages as drug delivery vehicles *in vivo*, it is important to take account of resident macrophages already present in the tumour and the circulation. Thus we now consider spheroid infiltration by two macrophage populations: inert, non-engineered macrophages (l_1) and active, engineered macrophages (l_2). We suppose that the evolution of both populations are governed by similar partial differential equations (see (25)), that they are subject to similar boundary and initial conditions (see (30) and (31)) and that the evolution of the tumour radius is governed by (35). Previous studies of macrophage trafficking indicate that systemically injected untransfected macrophages are outnumbered by resident host macrophages in tumours (Andreesen et al., 1998), which suggests that $l_{\infty 2} < l_{\infty 1}$. However, since intratumoural injection may be used to increase the number of modified macrophages reaching the tumour, the relative magnitudes of $l_{\infty 1}$ and $l_{\infty 2}$ may vary.

Figure 7(b) shows an example which mimics a possible experimental protocol, whereby a spheroid is initially grown in the presence of normal macrophages, these are then washed off at day 10 and replaced by modified macrophages for days 10 to 12, and then normal macrophages are again allowed to infiltrate the spheroid at the same time as tumour cell lysis is induced by the application of prodrug. We account for the finite period over which the engineered macrophages infiltrate the spheroid by writing

$$l_{\infty 1} = \begin{cases} 0 & t \in (10, 12) \\ l_{\infty 1} & \text{otherwise,} \end{cases} \qquad l_{\infty 2} = \begin{cases} l_{\infty 2} & t \in (10, 12) \\ 0 & \text{otherwise,} \end{cases} \qquad (36)$$

in equations (31) and (35). The example illustrated in the figure uses $l_{\infty 1} = l_{\infty 2} = 0.8$, and lysis is induced at $t = 12$ by setting $T_{on} = 12$ in equation (21).

From figure 7(b) we note that when the second macrophage population induces tumour cell lysis, the spheroid shrinks until the engineered macrophage level declines and growth resumes. Comparing figures 7(a) and (b), we note that when the engineered macrophages have to compete with inert macrophages, they attain lower levels than when they are the only macrophage population. Consequently, the reduction in tumour volume is less pronounced and shorter-lived.

5   Discussion

We have extended a continuum model of avascular spheroid growth originally developed by Ward and King (Ward and King, 1999), in order to study the impact of normal and engineered macrophages on such tumours. Both types of macrophages are assumed to migrate through the tumour by a combination of random motion and chemotaxis, the chemoattractant being produced by the tumour cells (and possibly macrophages) under hypoxia. The modified macrophages were assumed to stimulate tumour cell lysis under hypoxia.

By performing a series of numerical experiments we have compared the effect that normal (passive) and engineered macrophages have on the size and composition of the spheroids. For example, we found that the distribution of passive macrophages (i.e. macrophages which are incapable of killing tumour cells) within the tumour depends on the relative importance of chemotaxis and random motion, with greater localisation in the hypoxic region occurring when chemotaxis operates (compare figures 3(a) and (b)). Our simulations also show that on continuous infiltration by passive macrophages the limiting size of the spheroid is larger than when no macrophages are present (see figure 4), suggesting that the macrophages have a deleterious effect. On more detailed inspection we found that, while the overall tumour burden (i.e.

the number of tumour cells) increased when macrophages were present, the proportion of the spheroid volume occupied by tumour cells declined. Further, the proportion of tumour cells in the hypoxic region reduced markedly as they were displaced by the macrophages, thus making the tumour more responsive to standard chemotherapeutic agents that target proliferating cells. These contrasting points of view may contribute to uncertainty about the use of macrophage infiltration as a prognostic indicator.

In an attempt to simulate the action of macrophage-mediated therapies, we then considered the additional impact on the spheroid of macrophage-mediated tumour cell lysis. We chose to include this in a relatively simple fashion, mimicking the genetically engineered hypoxia induced production of substances inducing cell kill with an additional tumour cell death term dependent jointly on the macrophage and tumour cell density, with a rate increasing as nutrient levels decrease. This gives a biphasic response—a low lysis rate in the necrotic core since there are few macrophages and tumour cells there, a high rate in the hypoxic/quiescent layer, and a low rate in the proliferative rim since nutrient levels are high and thus lysis is not induced. As expected, continuous infiltration of such macrophages causes shrinkage, or at least slower growth, of tumour spheroids, with stronger responses as the maximum lysis rate is increased. Figure 6 shows that, as the lysis rate is increased, the tumour size decreases with diminishing effect. This is because the proportion of tumour cells falls to negligible levels, and there is little hypoxia to stimulate macrophage mediated lysis (data not shown). Maintaining a macrophage population at the tumour surface means there is a constant supply of macrophages, so that even if most of the tumour cells are killed, the spheroid volume is maintained. This would in fact correspond to effective elimination of the tumour. Figure 6 also illustrates that greater chemotaxis coefficients lead to spheroids with a larger diameter (due to increased macrophage accumulation), yet the fractional reduction in tumour size (relative to the untreated case with the same chemotactic parameter) is also increased. This again leaves the prognostic role of macrophage infiltration open to interpretation. More realistically, engineered macrophages would be delivered at intervals, rather than continuously, and simulations of this type demonstrate the role of mathematical modelling for the optimisation of repeated treatments.

Our model represents a first step towards the development of a more realistic model that will be used to predict the response of different tumour cell lines to macrophage-based therapies. Of the model extensions needed to achieve this goal, perhaps the most important is a more accurate description of the mechanism of action of particular therapeutic gene products. In this paper we have concentrated on killing tumour cells, a possibility that has been explored experimentally for the enzyme–prodrug pair cytochrome P450–Cyclophosphamide (Griffiths et al., 2000). Rather than the macrophages killing the tumour cells on contact at a rate which peaks

under hypoxia, as we assume here, in practice the modified macrophages express the enzyme under hypoxia. The enzyme then activates the prodrug, which is injected shortly after the macrophages. The active drug then diffuses and is taken up by the tumour cells, triggering cell death only when the cells attempt to proliferate. By combining the two-stage model of prodrug activation developed by Jackson et al. (Jackson et al., 1999; Jackson et al., 2000) with our model, we plan to include these additional details in a future model. Other strategies are possible, and could also be explored within our modelling framework. For example, macrophages could deliver replication-competent viral vectors to hypoxic tumour regions (Burke et al., 2002). Mathematical models for viral replication in tumour spheroids have been developed (Wu et al., 2001), and could be extended to include macrophage dynamics and macrophage-dependent viral delivery. Another issue that remains to be investigated concerns the response to combination therapies in which infusion with engineered macrophages alternates with administration of standard chemotherapeutic drugs. Of interest is the identification of the times at which therapies should be administered and their duration in order to optimise tumour treatment. Much of this future work will require more detailed parameter fitting to specific experimental situations.

Finally, by extending the model of vascular tumour growth developed by Breward et al. (Breward et al., 2003), we hope to predict the impact that genetically engineered macrophages can have on vascular tumours growing in vivo. In this case it will be important to take account of some of the pro-tumour functions that macrophages can perform. These include the production of angiogenic factors that stimulate the ingrowth of new blood vessels to the tumour (Folkman, 1974). Additional anti-tumour functions of the engineered macrophages that should then be considered include the production of anti-angiogenic chemicals and vascular targeting agents.

References

Anderson, A. R. A. and Chaplain, M. A. J. (1998). Continuous and discrete mathematical models of tumor-induced angiogenesis. *Bull. Math. Biol.*, 60(5):857–899.

Andreesen, R., Hennemann, B., and Krause, S. W. (1998). Adoptive immunotherapy of cancer using monocyte-derived macrophages: rationale, current status, and perspectives. *J. Leuk. Biol.*, 64:419–26.

Berg, H. C. and Purcell, E. M. (1977). Physics of chemoreception. *Biophys. J.*, 20:193–219.

Breward, C. J. W., Byrne, H. M., and Lewis, C. E. (2002). The role of cell-cell interactions in a two-phase model for avascular tumour growth. *J. Math. Biol.*, 45:125–152.

Breward, C. J. W., Byrne, H. M., and Lewis, C. E. (2003). A multiphase model describing vascular tumour growth. *Bull. Math. Biol.*, 65:609–640.

Burke, B., Sumner, S., Maitland, N., and Lewis, C. E. (2002). Macrophages in gene therapy: cellular delivery vehicles and in vivo targets. *J. Leuk. Biol.*, 72:417–428.

Byrne, H. M., King, J. R., McElwain, D. L. S., and Preziosi, L. (2002). A two-phase model of solid tumor growth. *App. Math. Lett.* in press.

Casciari, J. J., Sotirchos, S. V., and Sutherland, R. M. (1988). Glucose diffusivity in multicellular tumour spheroids. *Cancer Res.*, 48:3905–3909.

Drasdo, D. and Hohme, S. (2003). Individual-based approaches to birth and death in avascular tumors. *Math. Comp. Modelling*, 37(11):1163–1175.

Folkman, J. (1974). Tumour angiogenesis. *Adv. Cancer. Res.*, 19:331–358.

Fontelos, M. A., Friedman, A., and Hu, B. (2002). Mathematical analysis of a model for the initiation of angiogenesis. *SIAM J. Math. Anal.*, 33(6):1330–1355.

Franks, S. J. and King, J. R. (2002). Interactions between a uniformly proliferating tumour and its surroundings: uniform material properties. *IMA J. Math. App. Med. Biol.* Submitted.

Freyer, J. P. and Sutherland, R. M. (1983). Determination of apparent diffusion constants for metabolites in multicell tumour spheroids. *Adv. Exp. Med. Biol.*, 159:463–475.

Friedman, A. and Reitich, F. (1999). Analysis of a mathematical model for the growth of tumors. *J. Math. Biol.*, 38(3):262–284.

Greenspan, H. P. (1976). On the growth and stability of cell cultures and solid tumors. *J. Theor. Biol.*, 56:229–242.

Griffiths, L., Binley, K., Iqball, S., Kan, O., Maxwell, P., Ratcliffe, P., Lewis, C., Harris, A., Kingsman, S., and Naylor, S. (2000). The macrophage - a novel system to deliver gene therapy to pathological hypoxia. *Gene Therapy*, 7:255–262.

Hlatky, L., Suchs, R. K., and Alpen, E. L. (1988). Joint oxygen-glucose deprivation as the cause of necrosis in a tumour analogue. *J. Cell. Phys.*, 134:167–178.

Howell, W. M., Bateman, A. C., Turner, S. J., Collins, A., and Theaker, J. M. (2002). Influence of vascular endothelial growth factor single nucleotide polymorphisms on tumour development in cutaneous malignant melanoma. *Genes Immun.*, 3:229–232.

Ichikura, T., Tomimatsu, S., Ohkura, E., and Mochizuki, H. (2001). Prognostic significance of the expression of vascular endothelial growth factor (VEGF) and VEGF-C in gastric carcinoma. *J. Surg. Oncol.*, 78:132–137.

Jackson, T. L. and Byrne, H. M. (2002). A mechanical model of tumor encapsulation and transcapsular spread. *Math. Biosci.*, 180:307–328.

Jackson, T. L., Lubkin, S. R., and Murray, J. D. (1999). Theoretical analysis of conjugate localization in two-step cancer chemotherapy. *J. Math. Biol.*, 39:353–376.

Jackson, T. L., Senter, P. D., and Murray, J. D. (2000). Development and validation of a mathematical model to describe anti-cancer prodrug activation by antibody-enzyme conjugates. *J. Theor. Med.*, 2:93–111.

Kelly, C. E. (2002). *Mathematical modelling of macrophage-mediated therapy in cancer.* PhD thesis, University of Nottingham, Nottingham.

Kelly, C. E., Leek, R. D., Byrne, H. M., Cox, S. M., Harris, A. L., and Lewis, C. E. (2002). Modelling macrophage infiltration into avascular tumours. *J. Theor. Med.*, 4:21–38.

Leek, R. D. (1999). *The role of tumour associated macrophages in breast cancer angiogenesis.* PhD thesis, Oxford Brookes University, Oxford.

Levine, H. A., Pamuk, S., Sleeman, B. D., and Nilsen-Hamilton, M. (2001). Mathematical modeling of capillary formation and development in tumor angiogenesis: Penetration into the stroma. *Bull. Math. Biol.*, 63(5):801–863.

Lewis, J. S., Lee, J. A., Underwood, J. C. E., Harris, A. L., and Lewis, C. E. (1999). Macrophage responses to hypoxia: relevance to disease mechanisms. *J. Leuk. Biol.*, 66:889–900.

Lubkin, S. R. and Jackson, T. (2002). Multiphase mechanics of capsule formation in tumors. *J. Biomed. Eng.*, 124:237–243.

Maxwell, P. H., Dachs, G. U., Gleadle, J. M., Nicholls, L. G., Harris, A. L., Stratford, I. J., Hankinson, O., Pugh, C. W., and Ratcliffe, P. J. (1997). Hypoxia-inducible factor-1 modulates gene expression in solid tumors and influences both angiogenesis and tumorgrowth. *Proc. Nat. Acad. Sci. USA*, 94:8104–8109.

Owen, M. R. and Sherratt, J. A. (1997). Pattern formation and spatiotemporal irregularity in a model for macrophage-tumour interactions. *J. Theor. Biol.*, 189:63–80.

Scotton, C., Milliken, D., Wilson, J., Raju, S., and Balkwill, F. (2001). Analysis of CC chemokine and chemokine receptor expression in solid ovarian tumours. *Br. J. Cancer*, 85:891–897.

Sherratt, J. A. (1994). Chemotaxis and chemokinesis in eukaryotic cells: the Keller-Segel equations as an approximation to a detailed model. *Bull. Math. Biol.*, 56:129–146.

Sica, A., Saccani, A., Bottazzi, B., Bernasconi, S., Allavena, P., Gaetano, B., Fei, F., LaRosa, G., Scotton, C., Balkwill, F., and Mantovani, A. (2000). Defective expression of the monocyte chemotactic protein-1 receptor CCR2 in macrophages associated with human ovarian carcinoma. *J. Immunol.*, 164:733–738.

Sozzani, S., Luini, W., Molino, M., Jilek, P., Bottazzi, B., Cerletti, C., Matsushima, K., and Mantovani, A. (1991). The signal transduction pathway involved in the migration induced by a monocyte chemotactic cytokine. *J. Immunol.*, 147:2215–2221.

Ward, J. P. and King, J. R. (1997). Mathematical modelling of avascular tumour growth. *IMA J. Math. App. Med. Biol.*, 14:39–69.

Ward, J. P. and King, J. R. (1999). Mathematical modelling of avascular tumour growth II: Modelling growth saturation. *IMA J. Math. App. Med. Biol.*, 16:171–211.

Wiegel, F. W. (1983). Diffusion and the physics of chemoreception. *Phys. Rep.*, 95:284.

Wu, J. T., Byrne, H. M., Kirn, D. H., and Wein, L. M. (2001). Modeling and analysis of a virus that replicates selectively in tumor cells. *Bull. Math. Biol.*, 63:731–768.

A   Nondimensionalisation

Equations (1)-(5) are nondimensionalised using the following rescalings of space, time and all the dependent variables:

$$\mathbf{x}^* = \frac{\mathbf{x}}{R_m}, \quad t^* = p_m^{max} t, \quad \mathbf{v}^* = \frac{\mathbf{v}}{R_m p_m^{max}}, \quad R^* = \frac{R}{R_m} \tag{37}$$

$$l^* = \frac{l}{N_0}, \quad m^* = \frac{m}{N_0}, \quad n^* = \frac{n}{N_0}, \quad c^* = \frac{c}{c_\infty}, \quad a^* = \frac{a}{a_{char}}. \tag{38}$$

Here R_m is the radius of a single tumour cell, p_m^{max} is the maximum rate of proliferation of nutrient rich tumour cells, c_∞ is the nutrient concentration at the tumour surface, and a_{char} is a characteristic chemoattractant concentration. The corresponding parameter rescalings are:

$$d_l^*(c^*) = \frac{d_l(c)}{p_m^{max}} \quad p_m^*(n^*, c^*) = \frac{p_m(n, c)}{p_m^{max}}, \quad d_m^*(c^*) = \frac{d_m(c)}{p_m^{max}}, \tag{39}$$

$$d_c^*(l^*, m^*, c^*) = \frac{R_m^2 d_c(l, m, c)}{D_c c_\infty}, \quad p_a^*(l^*, m^*, c^*) = \frac{p_a(l, m, c)}{d_a a_{char}}, \quad d_a^* = \frac{R_m^2 d_a}{D_a}, \tag{40}$$

$$D_l^* = \frac{D_l}{p_m^{max} R_m^2}, \quad D_m^* = \frac{D_m}{p_m^{max} R_m^2}, \quad \chi^* = \frac{a_{char} \chi}{p_m^{max} R_m^2}, \tag{41}$$

$$D_n^* = \frac{D_n}{p_m^{max} R_m^2}, \quad D_c^* = \frac{D_c}{p_m^{max} R_m^2}, \quad D_a^* = \frac{D_a}{p_m^{max} R_m^2}. \tag{42}$$

$$h_l^* = \frac{h_l}{p_m^{max} R_m}, \quad l_\infty^* = \frac{l_\infty}{N_0}, \quad h_n^* = \frac{h_n}{p_m^{max} R_m}, \quad n_\infty^* = \frac{n_\infty}{N_0}, \quad h_a^* = \frac{h_a}{p_m^{max} R_m D_a}, \quad a_\infty^* = \frac{a_\infty}{a_{char}}. \tag{43}$$

After dropping $*$'s, these rescalings give equations (24,25) for the macrophage and tumour cell populations, and the following equations for nutrient and chemoattractant concentrations:

$$\frac{1}{D_c}\left[\frac{\partial c}{\partial t} + \frac{1}{r^2}\frac{\partial}{\partial r}\left[r^2 v c\right]\right] = \frac{1}{r^2}\frac{\partial}{\partial r}\left[r^2 \frac{\partial c}{\partial r}\right] - d_c(l, m, c) \tag{44}$$

$$\frac{1}{D_a}\left[\frac{\partial a}{\partial t} + \frac{1}{r^2}\frac{\partial}{\partial r}\left[r^2 v a\right]\right] = \frac{1}{r^2}\frac{\partial}{\partial r}\left[r^2 \frac{\partial a}{\partial r}\right] + d_a(p_a(l, m, c) - a), \tag{45}$$

and the chemoattractant boundary condition at the spheroid surface:

$$\frac{\partial a}{\partial r} - \frac{D_m}{D_a}\frac{a}{m}\frac{\partial m}{\partial r} = h_a(a_\infty - a) \quad \text{on } r = R(t). \tag{46}$$

Now we note that D_c and D_a characterise nutrient and chemoattractant diffusion in terms of cell radii squared per cell division cycle, which will be large. Thus $1/D_c$ and $1/D_a$ will be small parameters, and we may neglect terms involving these factors, to give quasi-steady equations for nutrient and chemoattractant concentrations. We then arrive at the system of equations (24)-(33).

Tables

Parameter	Dimensional Estimate	Dimensionless Estimate	Supporting references
R_0	80 μm	13	(Leek, 1999)
d_a	–	0.01	–
D_m	$5 \times 10^{-3} \mu$m^{2}s^{-1}	10	–
D_n	$10^{-1} \mu$m^{2}s^{-1}	500	(Ward and King, 1999)
D_l	5×10^{-3} μm^{2}s^{-1}	10	(Owen and Sherratt, 1997; Sozzani et al., 1991)
χ_l	2–6 $\times 10^{24}$ μm^{2}s^{-1}Mol^{-1}	500-2000	(Owen and Sherratt, 1997; Sozzani et al., 1991)
D_a	200 μm^{2}s^{-1}	-	(Owen and Sherratt, 1997)
D_c	50 μm^{2}s^{-1}	-	(Casciari et al., 1988; Freyer and Sutherland, 1983; Hlatky et al., 1988)
c_p	–	0.6	–
c_c	–	0.2	–
α	–	5	–
p_m^{max}	1 day^{-1}	1	(Kelly et al., 2002; Maxwell et al., 1997; Ward and King, 1999)
p_{am}^{max}	$10^{-25} d_a$ Mol μm^{-3}	1	(Owen and Sherratt, 1997; Sozzani et al., 1991)
p_{al}^{max}	–	variable	–
d_m^{max}	–	2	–
d_l^{max}	–	2	–
d_{cm}^{max}	–	0.005	(Ward and King, 1997)
d_{cl}^{max}	–	0.005	–
d_{cp}^{max}	–	0.01	–
k^{max}	–	variable	–
a_{char}	10^{-25} Mol μm^{-3}	1	(Owen and Sherratt, 1997; Sozzani et al., 1991)
h_l	–	2	–
h_n	–	100	–
h_a	–	0.01	–
l_∞	–	variable	–
n_∞	–	0.2	–
c_∞	–	1	–
a_∞	–	0	–
n_0	–	0.2	–

Table 1: A summary of the dimensional and dimensionless parameter estimates (see main text for details).

Figures & Legends
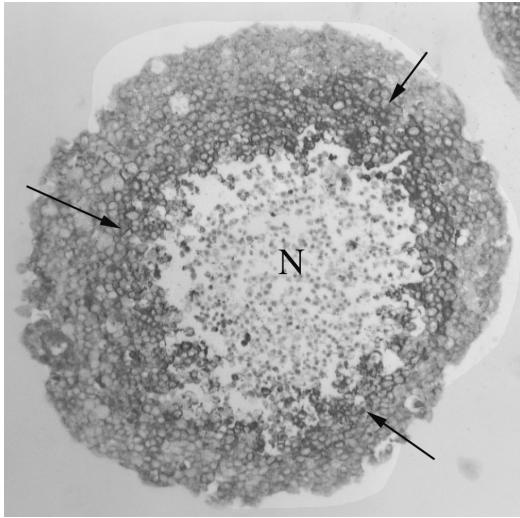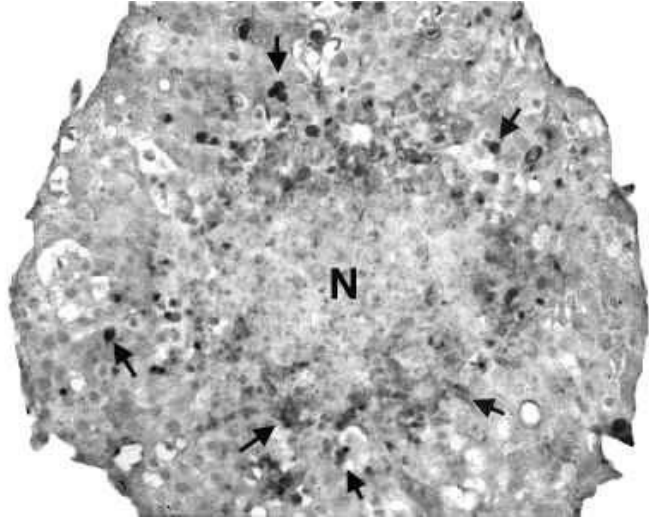
(a)   (b)

Figure 1: **(a)** Transverse section of a T47D Multicellular Tumour Spheroid, with a central necrotic area (N) of cell debris, surrounded by two layers of viable cells. The outer layer consists of normoxic cells, and the inner layer is hypoxic (dark staining is for the hypoxic marker, HIF-1α: see arrows). **(b)** Section of a human breast tumour spheroid, showing macrophage accumulation (dark staining, see arrows) in the inner hypoxic rim around the central necrotic area (N).
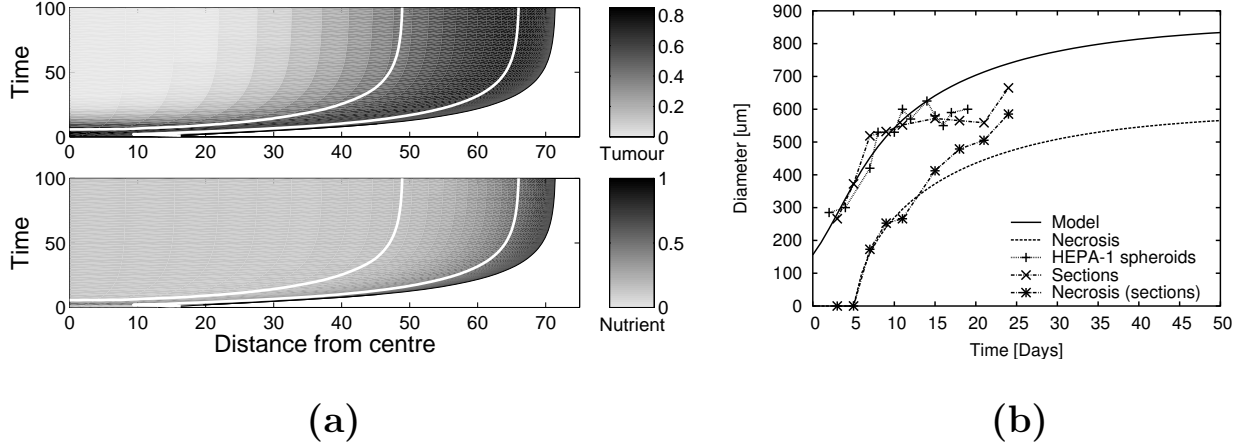
Figure 2: **(a)** Here we show how the tumour cells and nutrient concentration evolve when no macrophages are present ($l = 0$). The spheroid reaches an equilibrium size at which both the nutrient and tumour cell concentrations decrease with distance from the tumour boundary. At equilibrium the rate at which nutrient-rich cells near the boundary proliferate balances the rate at which nutrient-starved cells near the centre die. The solid white lines are contours of the nutrient concentration which define the positions of the hypoxic ($c = c_p = 0.6$) and necrotic ($c = c_c = 0.2$) boundaries. **(b)** Our model simulations are in good agreement with experimental data for the growth of HEPA-1 spheroids. The solid line represents the position of the outer tumour boundary and the dashed line the position of the necrotic boundary on which $c = c_c = 0.2$. Dimensional radii are shown in μm.

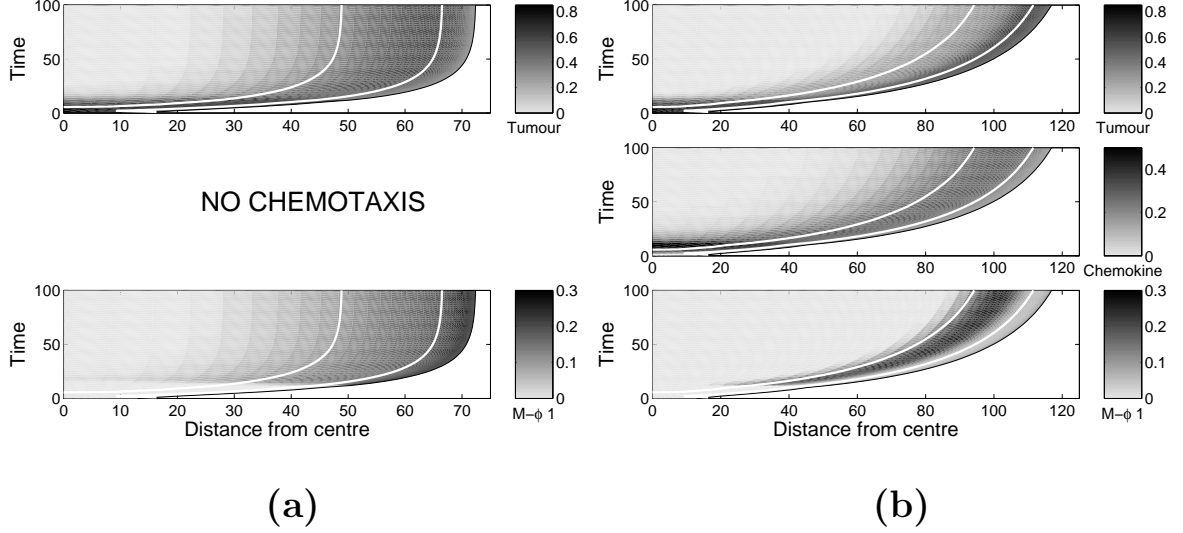**(a)**   **(b)**

Figure 3: Here we show how the spheroid's growth and composition are influenced by macrophage infiltration. The solid white lines are contours of c which define the positions of the hypoxic ($c = c_p = 0.6$) and necrotic ($c = c_c = 0.2$) boundaries. **(a)** Macrophages infiltrate by random motion alone ($\chi_l = 0$). In the absence of chemotaxis, the macrophages accumulate near the tumour boundary. The nutrient profile is qualitatively similar to that presented in Figure 2(a) and is, therefore, omitted. **(b)** Macrophages which infiltrate by random motion and chemotaxis, the chemoattractant being produced by the tumour cells alone With chemotaxis, the macrophages localise in the hypoxic region, where the chemokine concentration is largest. The solid white lines define the positions of the hypoxic and necrotic boundaries.
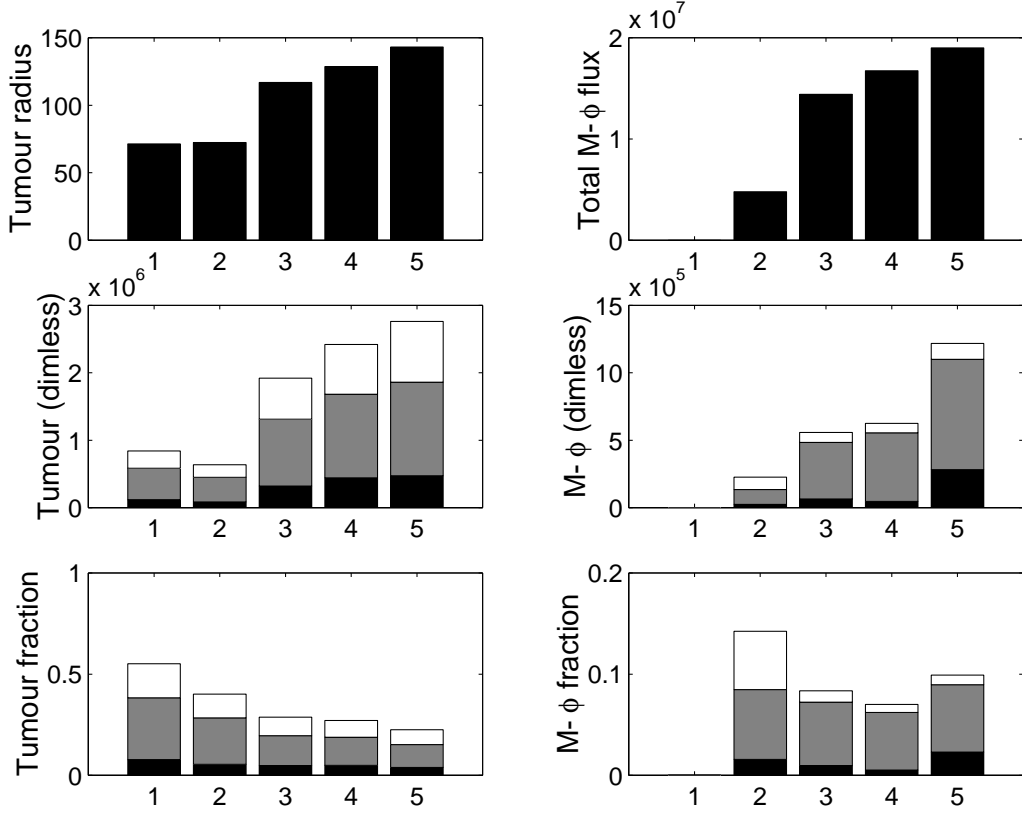
Figure 4: Here we present a series of figures showing how the spheroid's size and composition at $t = 100$ depend on the mechanisms by which the macrophages infiltrate and their death rate. The bottom four panels provide information on the tumour's composition, each vertical bar being subdivided according to the proportion in the proliferating (white), quiescent (shaded) and necrotic (black) regions of the spheroid. Key: (1) Control (no macrophages present); (2) macrophages infiltrate by random motion alone; (3) macrophages infiltrate by random motion and chemotaxis, with only the tumour cells producing chemoattractant; (4) as for (3), but with the macrophages also producing chemoattractant; (5) as for (3), but with the macrophage death rate halved ($d_l^{max} = 1$).
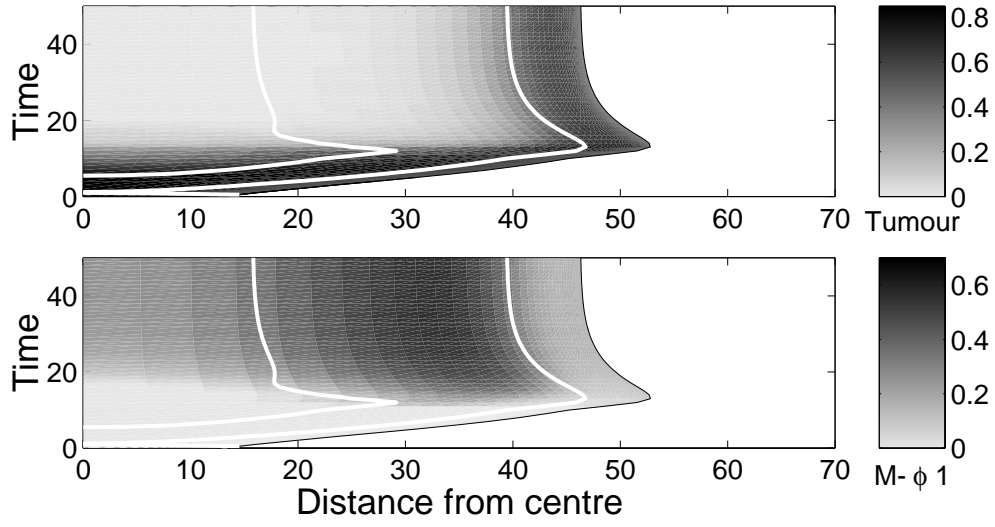
Figure 5: Here we show how the tumour shrinks, but is not eliminated, when it is infiltrated with macrophages that stimulate tumour cell death at a rate which peaks under hypoxia. The macrophages are continuously infused from $t = 10$ whereas macrophage-mediated tumour cell lysis with $k^{max} = 6$ is not initiated until the prodrug is administered at $t = 12$. The solid white lines define the positions of the hypoxic and necrotic boundaries.
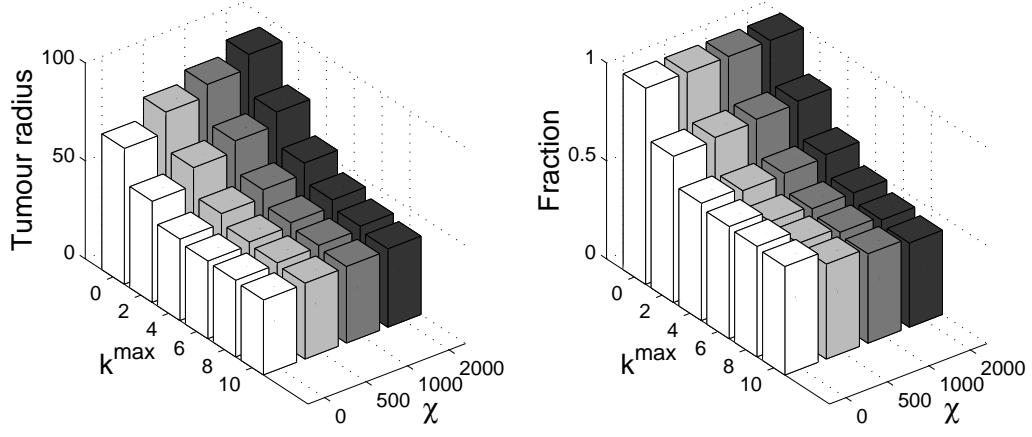
Figure 6: Here we show the reduction in spheroid size at $t = 40$ as the maximum lysis rate, k^{max}, and chemotaxis coefficient χ vary. As k^{max} increases, the spheroid radius decreases with diminishing effect. When k^{max} is large the tumour cell fraction decreases to almost insignificant levels (data not shown), and varying macrophage chemotaxis makes little difference. Whilst spheroids with chemotactically infiltrating macrophages are larger, the fractional reduction in size induced by lysis is greater.
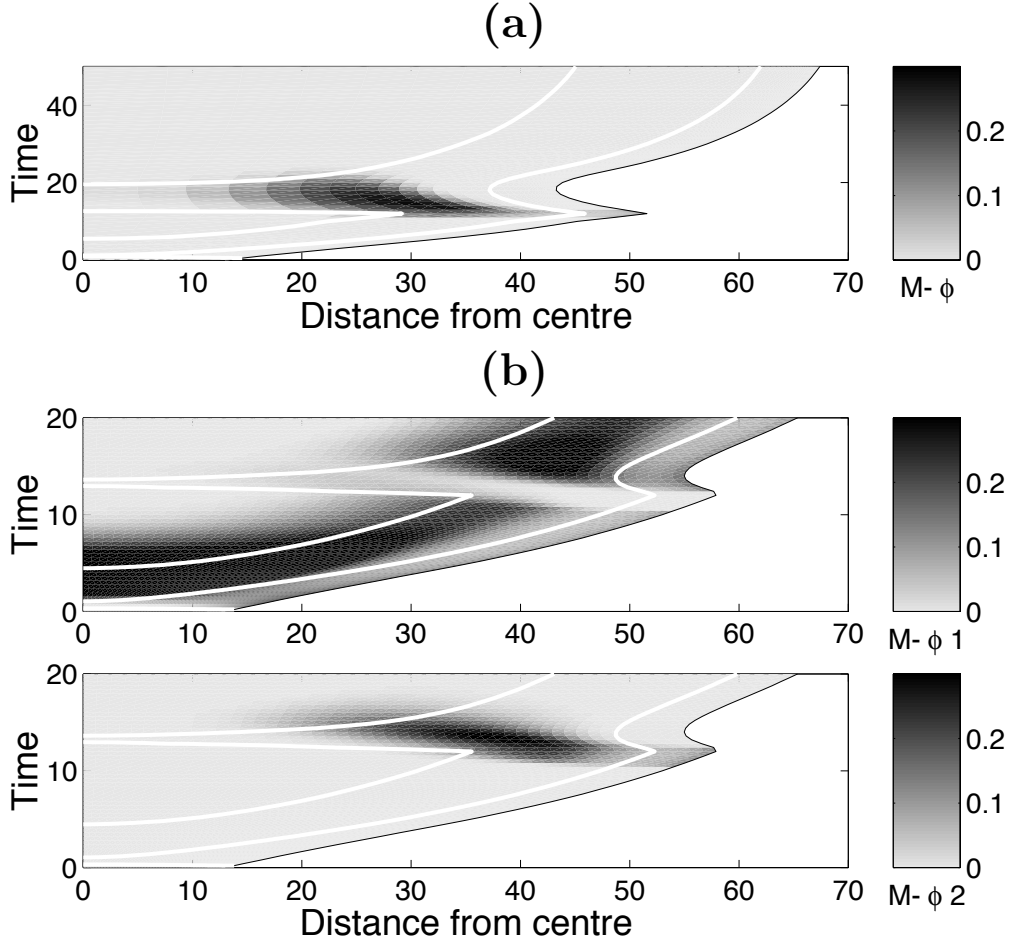
Figure 7: Here we show how the application of modified macrophages for a finite period affects the spheroid's growth. **(a)** A single population of macrophages is infused into the spheroid from $t = 10$ to $t = 12$, and tumour cell lysis with $k^{max} = 20$ is switched on at $t = 12$. The macrophages migrate towards the hypoxic region and the spheroid shrinks until the macrophage level there declines and growth resumes. **(b)** Multiple macrophage populations with the second infiltrating "engineered" population inducing tumour cell lysis under hypoxia. Parameter values were $l_{\infty 1} = l_{\infty 2} = 0.8$ in equation (36), $k^{max} = 20$. The engineered and inert macrophages compete for space, and the reduction in tumour volume is therefore less pronounced and shorter-lived. The solid white lines define the positions of the hypoxic and necrotic boundaries.